applied sciences

MDPI

Article

Bonding Performance of Steel Rebar Coated with Ultra-High-Performance Concrete

In-Hyeok Eom [1], Sang-Keun Oh [2] and Byoungil Kim [2,*]

[1] Convergence Institute of Biomedical Engineering and Biomaterials, Seoul National University of Science & Technology, 232 Gongneung-ro, Nowon-gu, Seoul 01811, Korea; eom084@kict.re.kr

[2] School of Architecture, Seoul National University of Science & Technology, 232 Gongneung-ro, Nowon-gu, Seoul 01811, Korea; ohsang@seoultech.ac.kr

* Correspondence: bikim@seoultech.ac.kr; Tel.: +82-2-970-6512

Featured Application: The improvement of the bond performance between reinforcing bars and the concrete matrix with a thin coating of ultra-high-performance concrete (UHPC).

Abstract: In this study, to improve the bond performance of reinforcing bars fixed inside concrete, a pullout test using ultra high-performance concrete (UHPC) and structural steel fibers was conducted and a model that could predict the performance was also presented. After creating a UHPC layer on the rebar surface, the specimens were prepared along with three types of structural fibers. The structural fibers with different shapes were mixed up to 0.2%, 0,4%, 0.6%, 0.8%, 1% and 2% to analyze their effects on the bond failure at the interface. As a result of the experiment, the pullout resistance ability of the specimen thinly coated with UHPC maintained high residual stress due to the steep section reaching the maximum load, increased the maximum pullout load, and delayed the bond failure during the extraction process. As a result of the cross-sectional examination of the specimen, the coating of UHPC was strongly attached to the rebar surface and the bond surface was broken through sliding at the interface (UHPC–ordinary Portland concrete (OPC)). It was found that the increase in the structural fiber significantly improved the pulling-out resistance at the interface. The proposed model based on the existing Cosenz–Manfredi–Realfonzo (CMR) and Bertero–Popov–Eligehausen (BPE) prediction models was found to be in good agreement with the experimental results.

Keywords: UHPC; interface; pullout; coating; steel fiber; steel rebar

check for updates

Citation: Eom, I.-H.; Oh, S.-K.; Kim, B. Bonding Performance of Steel Rebar Coated with Ultra-High-Performance Concrete. *Appl. Sci.* **2022**, *12*, 6808. https://doi.org/10.3390/app12136808

Academic Editors: Peng Liu and Ying Chen

Received: 25 May 2022
Accepted: 29 June 2022
Published: 5 July 2022

1. Introduction

Reinforced concrete is a structure with sufficient strength and stiffness for various loads due to its excellent bonding strength between the concrete as the compression member and the rebar as the tensile member [1]. Due to the strong alkalinity of concrete, a passivation film is formed on the surface of the reinforcing bar to prevent fatal corrosion to the structure over a long period of time, while maintaining excellent adhesion to the rebar [2]. In particular, cracks occurring in the tensile part of reinforced concrete lower the stiffness of the member and induce the redistribution of internal stress. [3]. In order to delay the progress of cracks occurring at the interface between the reinforcing bars and the concrete and to maintain the integrity for a long time, it is necessary to form a sufficient bond at the interface. The bond properties at the interface are determined by the crack width, crack spacing, and tension-stiffening phenomenon occurring in the concrete cross-section, as well as the roughness of the attachment surface and the strength of the member [3,4]. The bond stress, which is the shear stress acting along the reinforcing bar and the concrete surface, is transmitted to the concrete via chemical adhesion at the interface, friction, and the interlocking action between the nodes of the deformed rebar [5–9]. As a result, the sufficient bonding ability at the interface is one of the very important aspects in the structural behavior of reinforced concrete members. Insufficient bond capacity causes bending and deterioration of the shear performance, leading to premature failure of the structure [10].

With the continuous research and development (R&D) of concrete engineering technology, the number of cases involving the field application of ultra-high-performance concrete (UHPC) has been increasing recently [11–17]. Ultra-high-performance concrete has excellent strength (compressive strength of 150 MPa or more and tensile strength of 8 MPa or more) among the existing concretes, excellent ductility due to the mixing of steel fibers, low permeability of harmful substances due to minimized internal voids (high durability), and excellent material fracture performance [18–26]. It has strain-hardening characteristics, inducing multiple micro-cracks by mixing the steel fibers after cracking the concrete under maximum load, meaning it can be applied to various structures [27]. The study to improve the bond performance of ultra-high-performance concrete with steel or FRP bars was conducted by applying them to I-girders and deck joints, confirming their potential as tensile and flexural materials [28–31]. GFRP rebar does not corrode, has an excellent relative strength-to-weight ratio, and is used as a substitute for existing rebar due to its low-shrinkage stress generation. However, there is a disadvantage in that the redistribution of stress during the drawing process is not smooth due to the relatively low bond strength compared to reinforcing bars [32–35]. By replacing the concrete matrix with UHPC, a study was also conducted to improve the adhesion strength and ductility, with strong adhesion performance for the GFRP reinforcing bars, confirming the improvement of the adhesion–slip behavior due to the application of UHPC [36–38].

Although very positive research results have been confirmed for the application of UHPC to improve the performance of reinforced concrete structures, the economic feasibility is also an essential factor for its wide application in construction sites. Due to the material composition of UHPC, which is up to several times more expensive than general concrete, it has limited application in the field. In this study, a strong bond with the rebar was induced by thinly coating UHPC on the attachment surface of the rebar using the spray method. After forming a coating film on the rebar surface, general concrete was poured to reinforce the bonding interface between the UHPC and concrete and pullout tests were conducted. In addition, in order to further improve the redistribution of stress on the bond surface, three types of structural steel fibers were mixed up to 1% to check the bond–slip behavior. Finally, an analysis model that can predict the bond–slip behavior compared to the existing model was suggested.

2. Materials and Methods

2.1. Materials

In this study, steel rebars with a diameter of 12.7 mm, specific gravity of 7.9 g/cm^3, yield strength of 410 MPa, fracture strength of 560 GPa, and modulus of elasticity of 200 GPa were used. As shown in Figure 1, the UHPC was coated on the surface of the steel rebar with a thickness of about 2 to 3 mm to prepare for the pullout test. The UHPC used for the steel rebar coating consisted of the mixing ratio shown in Table 1 and was applied with a spray gun. By coating the UHPC with the characteristics of high flow and ultra-high-strength on the surface of the rebar, an interfacial area between the concrete matrix and the rebar was newly created to induce a change in the interfacial bonding mechanism compared to the existing one.

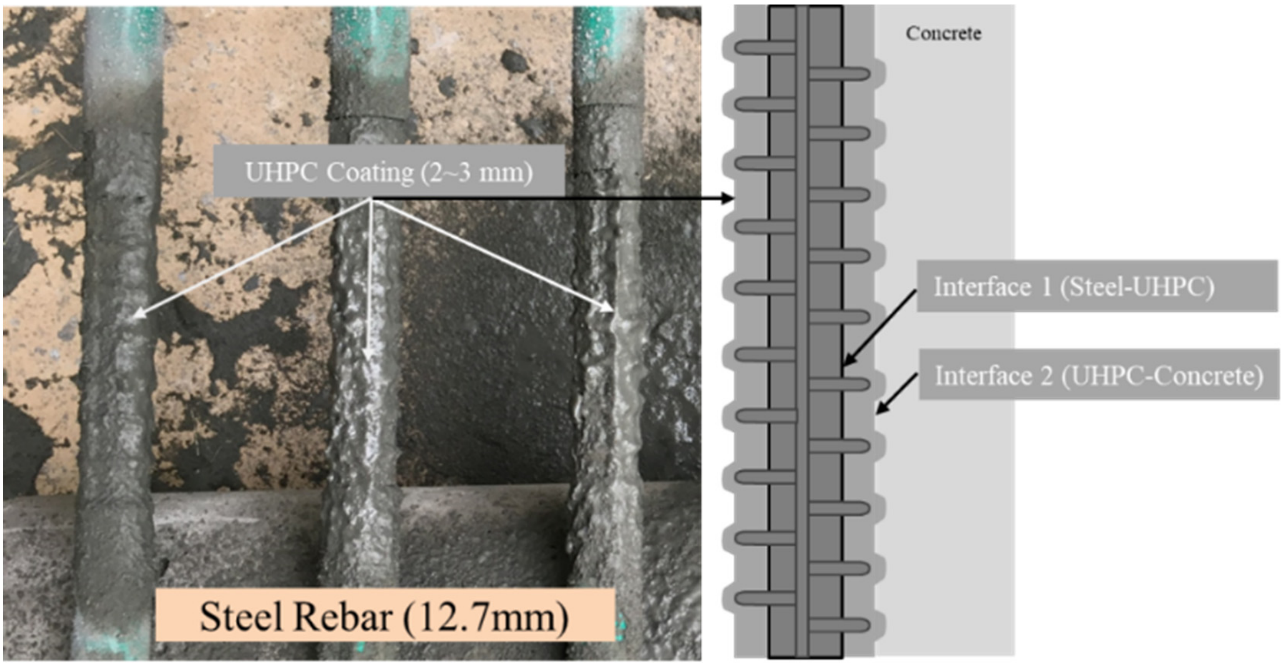

Figure 1. Steel rebar coated with UHPC.

Table 1. Ultra-high-performance concrete mix proportions.

Specimen	W/C (%)	Unit Weight (kg/m^3)						
		Water	Cement	Silica Fume	Silica Sand	Filler	Super Plasticizer	Anti-Foamer
UHPC	30	235	784	196	862	235	47.0	2.35

Table 2 shows the physical properties of the three types of steel fibers (K-steel Manufacturing Company) mixed in the concrete matrix and of the reference PVA fibers for comparison [32]. The test results for the PVA fibers without the UHPC coating on the reinforcing bars were added in order to compare the effects of the stiffness and bond strength on the load–slip curves. For all three types, the aspect ratio (L/D) was set to 70 to check the difference in performance according to the surface structure of the steel fibers. The hooked steel fiber had a tensile strength of 1300 MPa and a curved end. The crimped steel fiber had a tensile strength of 2900 MPa and the crimped stainless-steel fiber had a tensile strength of 1950 MPa, which was considerably larger than that of HSF. The process of manufacturing crimp-type fibers was in the order of a hydrochloric acid bath, water washing, a bonderite bath, water washing, a neutralization bath, a bonderizing bath, a lime bath, and drying. The primary pickling film (CA, BCA) removes the scales from the surface, improves the wire drawing process, and prevents rust, with lime film being the main type. The secondary pickling film (BRL, BCA) improves the drawing ability by removing the scales generated during the heat treatment on the wire's surface. In particular, phosphate and lubricant coatings are the main types of coatings used to prevent the adhesion that occurs during cold-press processing. The final process, the drawing process, is a manufacturing process that makes wires of a desired shape and dimensions by passing the wire through the holes in the die during production, and this process is repeated to produce the final product. Two types of concrete were used for all specimens. The average compressive strength of the concrete with HSF, CSF, and CSSF was 23.3 MPa, while that of the 1% PVA fiber was 61 MPa and that of the 2% PVA fiber was 58 MPa. Although the addition of fibers produced a slight change in compressive strength, the difference between the control and fiber specimens was not significant [32].

Table 2. The properties of different fibers.

Variables	**Hooked Steel Fiber (HSF)**	**Crimped Steel Fiber (CSF)**	**Crimped Stainless Steel Fiber (CSSF)**	**Polyvinyl Alcohol Fiber (PVA)**
Length (mm)	35	35	35	8
Diameter (mm)	0.5	0.5	0.5	40 (μm)
Aspect Ratio (L/D)	70	70	70	-
Surface Structure	Hooked-end	Crimped	Crimped stainless	Resin-bundled chopped
Density (g/cm^3)	7.8	7.8	7.8	1.3
Tensile strength (MPa)	1300	2900	1950	1300
Shape	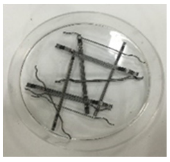			

2.2. Specimens for Pullout Test

The specimen size for the pullout test was 190.5 × 102 × 152.4 mm^3 modified from the experimental investigation performed by Alavi-Fard et al. [39]. Each specimen was made up of a concrete cube with a UHPC-coated steel rebar embedded horizontally along a central axis, as shown in Figure 2, with mixing proportions shown in Table 3.

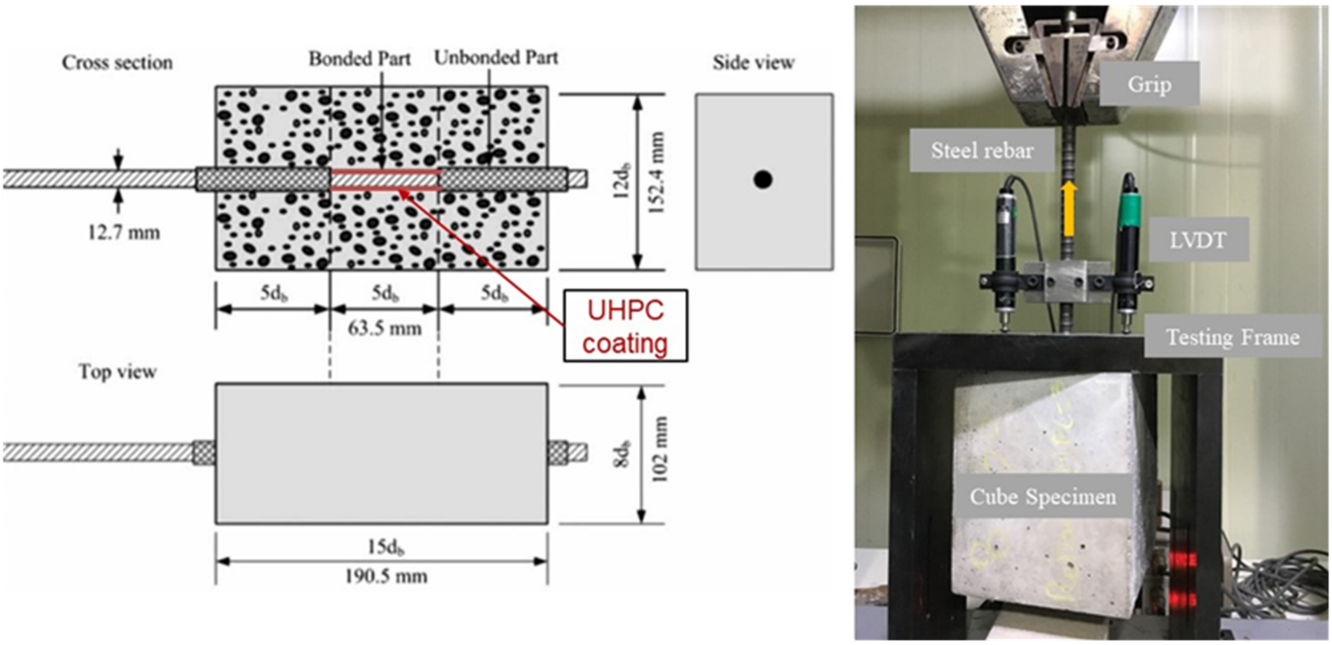

Figure 2. Specimen and testing setup.

The bond length of the embedded rebar was set to 63.5 mm, five times the diameter of the rebar. Furthermore, in order to make an effective measurement of the interfacial bonding behavior on the bonded length, the rebar on the top and bottom sides was sheathed with a soft PVC tube to prevent bonding between the bar and the concrete. Therefore, only the bond strength of the rebar near the center of the specimen was measured. The specimens shown in Table 4 were prepared. Fresh concrete was placed in two layers and each layer was rodded with a tamping rod and table vibrator. The concrete was cast horizontally with the UHPC-coated steel rebar inside the steel formwork. After molding, the specimens were instantly covered with a plastic sheet, stopping moisture loss for at least 48 h. The specimens were then removed from their molds and continuously cured underwater until testing at 21 °C. In this investigation, we mainly considered the response of the surface treatment of UHPC-coated steel rebars combined with structural fibers to pullout loading on the interfacial zone.

Table 3. Concrete mix proportions.

Mix Type	Cement (kg/m^3)	Water (kg/m^3)	Sand (kg/m^3)	Coarse Aggregate (kg/m^3)	Blast Furnace Slag (kg/m^3)	Fly Ash (kg/m^3)	Fiber Content (kg/m^3)	Super-Plasticizer (kg/m^3)
21-N (OPC)	239	164	922	928	30	30	-	1.79
Steel-1 (PVA0)	580	255	580	-	-	580	0	6.96
Steel-2 (PVA1)	580	255	580	-	-	580	13	6.96
Steel-3 (PVA2)	580	255	580	-	-	580	26	11.6
21-C-0.2-SF	239	164	922	928	30	30	0.31	1.79
21-C-0.4-SF	239	164	922	928	30	30	0.63	1.79
21-C-0.6-SF	239	164	922	928	30	30	0.94	1.79
21-C-0.8-SF	239	164	922	928	30	30	1.26	1.79
21-C-1.0-SF	239	164	922	928	30	30	1.57	1.79

Table 4. Specimens in the pullout test.

Mix Type	Fiber Volume Fraction, V_f (%)	Specimen Name for Pullout Test
21-N (OPC)	None	21-N
Steel-1 (PVA0)	None	PVA 0%
Steel-2 (PVA1)	1%	PVA 1%
Steel-3 (PVA2)	2%	PVA 2%
21-C(UHPC coating)	None	21-C
21-C-SF-A	0, 0.2, 0.4, 0.6, 0.8, 1.0	21-C-V_f-HSF
21-C-SF-B	0, 0.2, 0.4, 0.6, 0.8, 1.0	21-C-V_f-CSF
21-C-SF-C	0, 0.2, 0.4, 0.6, 0.8, 1.0	21-C-V_f-CSSF

2.3. Test Setup and Testing Procedure

The specimen was placed on the universal testing machine (UTM) so that the surface of the cube specimen on the side of the long end of the bar was in contact with the bottom of the mold. The end of the rebar was gripped using the jaws of the testing machine, as shown in Figure 2. The pullout behaviors of the UHPC-coated steel rebar were identified using a 2000-kN-capacity universal testing machine. A rate of 0.02 mm/s was selected and a continuous pullout load was first applied to the bars until failure. The interfacial bond slip between the embedded rebar and the concrete at the loaded end was simultaneously measured using linear variable displacement transducers (LVDTs). The readings of the applied pullout load and the corresponding three LVDTs were automatically recorded through a data logger.

3. Results and Discussion

The compressive strength of the UHPC presented in Table 1 was evaluated from a total of 5 specimens. Among them, the average values of the three specimens were calculated after excluding two specimens with a standard deviation of 5% or more of the compressive strength. After curing, the average compressive strength on the 28th day was 145.3 MPa. The ultra-high-strength UHPC was coated on the surface of the reinforcement to a certain thickness, and in addition a new type of interface was formed with the general concrete mixed with three types of steel fibers. Composite pullout resistance capability was expected at the newly formed interface 1 and interface 2.

Except for the specimen with high CSF and CSSF ratios, all specimens showed pullout failure before the yielding of rebars, without splitting cracks appearing on the surfaces of the specimens. The specimens with 0.8% and 1% of CSF or CSSF showed pullout failure after the yielding of rebars. The interfacial debonding behaviors of the pullout test specimen consisting of UHPC-coated steel rebar and different structural fibers on the interfacial bonding zone are discussed in this section. The pullout failure of the rebars was defined when the applied load reached the maximum point. The corresponding values of the maximum nominal bond stress and slip were then determined. Since the interfacial stress distribution between the rebar and concrete matrix was not constant along the embedded part, the average bond strength was calculated as follows:

$$\tau_{max} = \frac{P_{max}}{\pi d_b l_b} \tag{1}$$

where τ_{max} is the bond strength, P_{max} is the maximum tensile load, d_b is the rebar diameter, and l_b is the embedment length. The various test specimens' performances as a result for the pullout test are summarized in Table 5. In this table, f'_c is the concrete strength used for making pullout specimens, τ_{max} is the bond strength, and S_m is the slip value at the maximum load. The mean values of the bond strength and the slips are summarized in the table. The normalized bond strength(τ^*_{max}) [32–35] describing the effect of concrete strength was calculated as follows:

$$\tau^*_{max} = \frac{\tau_{max}}{\sqrt{f'_c}} \tag{2}$$

Table 5. Experimental results for pullout test specimens.

Specimen	P_{max} (kN)	τ_{max} (MPa)	$\tau_{\text{max-mean}}$ (MPa)	S_m (mm)	$S_{\text{m-mean}}$ (mm)	τ^*_{max} (MPa)	Failure Mode
21-N-1	39.71	15.68	15.40	1.64	1.63	3.26	PO
21-N-2	38.30	15.12		1.62		3.14	PO
21-C-1	45.24	17.87	17.76	1.79	1.74	3.71	PO
21-C-2	44.70	17.65		1.68		3.66	PO
PVA0S1 **	69.64	27.50		0.50		3.55	PO
PVA0S2 **	70.40	27.80	27.27	0.80	0.60	3.59	PO
PVA0S3 **	67.10	26.50		0.50		3.42	PO
PVA1S1 **	71.16	28.10		1.30		3.59	PO
PVA1S2 **	73.18	28.90	28.80	1.00	1.20	3.70	PO
PVA1S3 **	74.45	29.40		1.30		3.76	PO
PVA2S1 **	77.74	30.70		1.50		4.03	PO
PVA2S1 **	76.47	30.20	30.73	1.60	1.10	3.97	PO
PVA2S1 **	79.26	31.30		1.20		4.10	PO
21-C-0.2-HSF-1	46.39	18.32	18.56	2.27	2.22	3.80	PO
21-C-0.2-HSF-2	47.60	18.80		2.16		3.90	PO
21-C-0.4-HSF-1	49.54	19.56	19.44	1.44	1.41	4.06	PO
21-C-0.4-HSF-2	48.90	19.31		1.38		4.01	PO
21-C-0.6-HSF-1	50.63	20.00	20.15	1.92	1.86	4.15	PO
21-C-0.6-HSF-2	51.40	20.30		1.80		4.21	PO
21-C-0.8-HSF-1	52.86	20.88	20.75	1.52	1.49	4.33	PO
21-C-0.8-HSF-2	52.20	20.61		1.47		4.28	PO
21-C-1.0-HSF-1	53.33	21.06	21.11	1.81	1.80	4.37	PO
21-C-1.0-HSF-2	53.60	21.17		1.78		4.40	PO

Table 5. *Cont.*

Specimen	P_{max} (kN)	τ_{max} (MPa)	$\tau_{\text{max-mean}}$ (MPa)	S_{m} (mm)	$S_{\text{m-mean}}$ (mm)	τ^{*}_{max} (MPa)	Failure Mode
21-C-0.2-CSF-1	49.77	19.65	19.78	1.43	1.44	4.08	PO
21-C-0.2-CSF-2	50.40	19.90		1.45		4.13	PO
21-C-0.4-CSF-1	51.96	20.52	20.84	1.15	1.17	4.26	PO
21-C-0.4-CSF-2	53.60	21.17		1.18		4.40	PO
21-C-0.6-CSF-1	58.54	23.12	22.89	1.75	1.80	4.80	PO
21-C-0.6-CSF-2	57.40	22.67		1.84		4.71	PO
21-C-0.8-CSF-1	57.38	22.66	22.90	0.81	0.80	4.70	SY
21-C-0.8-CSF-2	58.60	23.14		0.79		4.80	SY
21-C-1.0-CSF-1	62.39	24.64	24.86	0.87	0.88	5.12	SY
21-C-1.0-CSF-2	63.50	25.08		0.90		5.21	SY
21-C-0.2-CSSF-1	46.70	18.44	18.66	0.53	0.52	3.83	PO
21-C-0.2-CSSF-2	47.80	18.88		0.51		3.92	PO
21-C-0.4-CSSF-1	51.86	20.48	20.72	1.18	1.20	4.25	PO
21-C-0.4-CSSF-2	53.10	20.97		1.23		4.35	PO
21-C-0.6-CSSF-1	54.46	21.51	21.77	1.83	1.88	4.47	PO
21-C-0.6-CSSF-2	55.80	22.04		1.92		4.58	PO
21-C-0.8-CSSF-1	58.98	23.29	23.02	1.23	1.20	4.84	SY
21-C-0.8-CSSF-2	57.60	22.75		1.18		4.72	SY
21-C-1.0-CSSF-1	58.27	23.01	23.19	0.70	0.72	4.78	SY
21-C-1.0-CSSF-2	59.20	23.38		0.73		4.85	SY

PO: pull out failure; SY: steel yield failure; τ^{*}_{max} normalized bond strength; ** reference [32] test results.

Even if the maximum load of the specimens with PVA is greater than that of the other specimens because of the difference in concrete strength, the normalized bond strengths (τ^{*}_{max}) of the specimens with normal or high-strength concrete will be similar.

3.1. Load–Slip Relationship

Figure 3 shows the load–slip curve for specimens 21_N containing a reinforcing bar without the UHPC coating and 21_C containing a reinforcing bar with the UHPC coating. When comparing the uncoated test specimen (21_N) with the UHPC-coated test specimen (21_C), noticeable changes (bond strength, toughness) in the coated test specimen can be confirmed. The load–slip curves of the two types of specimens were similar. A small slip change was shown in the initial loading section, and after reaching the maximum load the load gradually decreased, with the slip increasing. However, the bond strength of 21_C was 15.3% greater than that of 21_N and resulted in an increase in toughness performance. This was because the UHPC coating creates an additional interface and increases the bonding strength between the rebar and concrete, thereby delaying the progress of cracks. Figure 4 shows the load–slip curve of the uncoated rebars in concrete mixed with the PVA fiber. When the fibers were mixed, the slip resulted in the initial load section being smaller. As shown in Figure 4, the fiber increased the bond strength of the rebars, but not by much. The bond strength of specimens with 1% and 2% PVA fiber increased by about 6% and 13.1%, respectively, which were lower than the increases due to the UHPC coating.

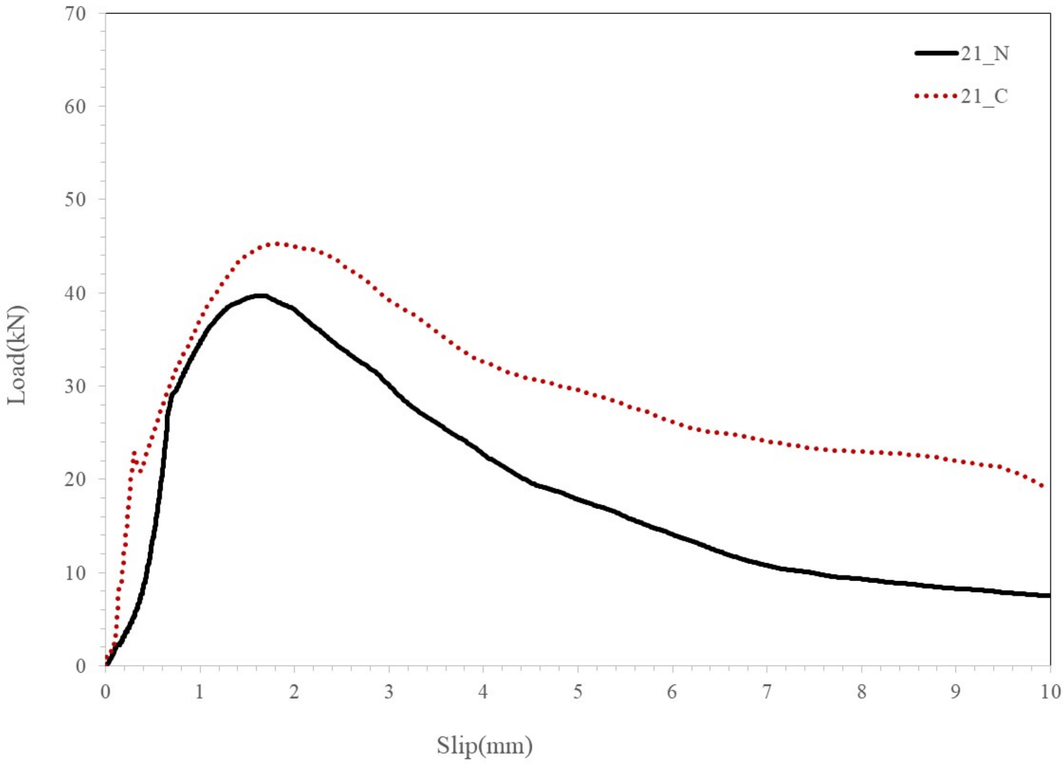

Figure 3. Load–slip curves with and without UHPC coating.

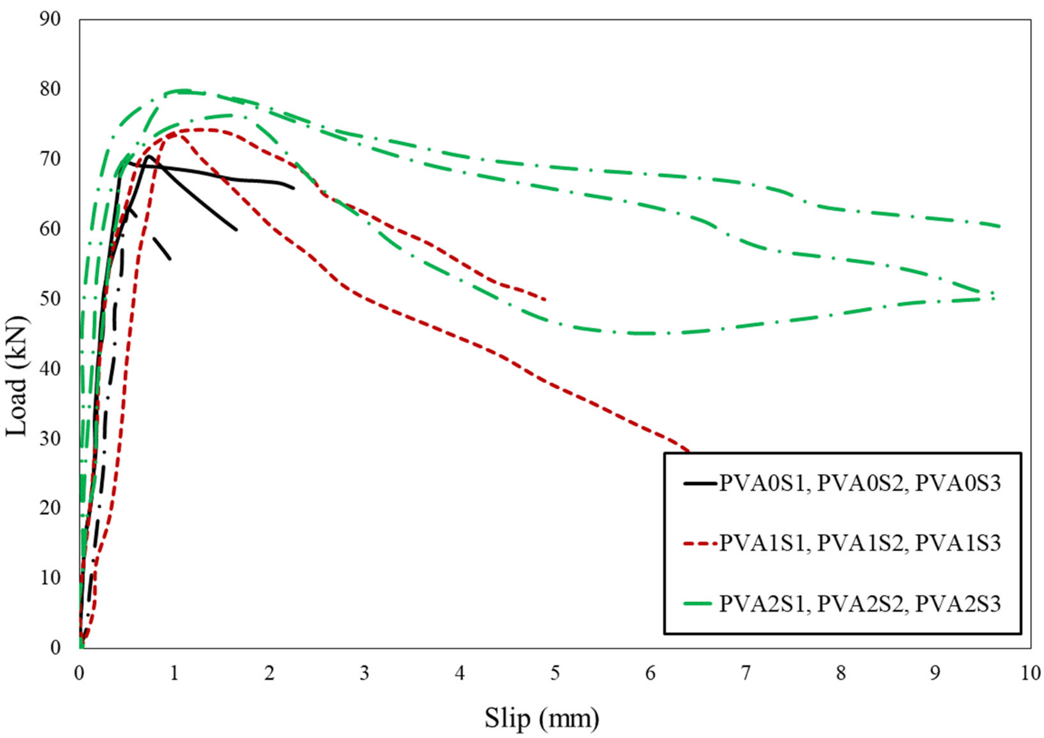

Figure 4. Load–slip curves of uncoated rebars with PVA fiber [32].

Figure 5 shows the load–slip curve for a pullout test specimen using concrete mixed with hooked steel fibers (HSF) in a reinforcing bar coated with UHPC. The load–slip curve of the test specimen in which 0.2–1.0% of HSF was mixed in the concrete matrix showed a more evident resistance improvement on the adhesion surface when the UHPC was coated. With a small slip, the initial ascent section increased very steeply and showed a softening of the load reduction after reaching the maximum load. In the test specimens containing 0.6% and 0.8% HSF, rapid adhesion failure between the rebar and concrete interface was shown in the softening process. It can be seen that the behavior up to adhesion failure was affected by the frictional resistance caused by the strong chemical adhesion between interface 1 (concrete matrix-UHPC interface) and interface 2 (UHPC-rebar interface). It was found that the maximum load value corresponding to the adhesion failure increased and the energy dissipation ability was also improved due to the increase in fiber mixing.

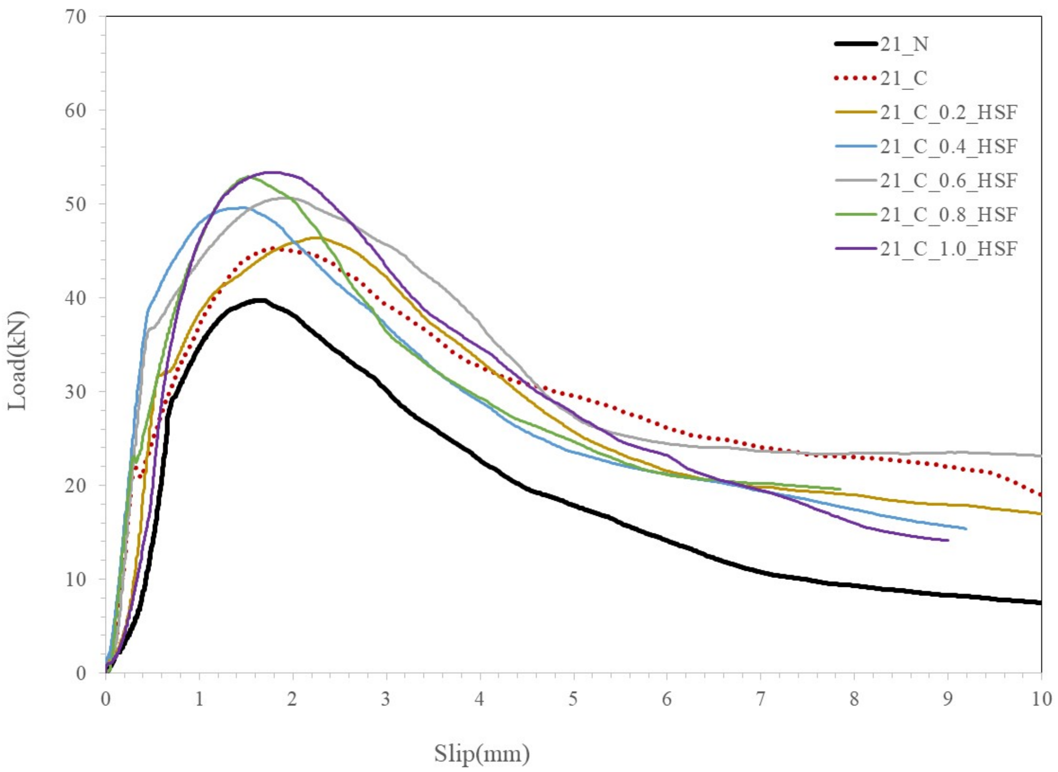

Figure 5. Load–slip curves with hooked-end steel fiber.

Figure 6 shows the results of the pullout test for rebar coated with UHPC after mixing CSF fibers in the concrete matrix. Similar to the case for HSF, the initial section shows a steep load increase accompanied by a small slip due to the strong bonding force at the interface. Increasing the mixing amount of fibers tends to gradually decrease the load after reaching the maximum load, while causing a steeper rise section. When the mixing ratio of CSF was 0.8% or more, the yield phenomenon of the rebar occurred in the maximum load section. It was judged that the yield phenomenon of the reinforcing bar occurred because the bonding ability at the interface was larger than that of the reinforcing bar itself [40]. In particular, the specimens mixed with 1% CSF showed a pullout failure phenomenon from the concrete matrix after slipping over a long section of the yield area of the reinforcing bar. Figure 7 shows the load–displacement curves of the test specimen mixed with CSSF fibers. Compared with Figure 5, the overall tendency was similar, and the yield phenomenon of the rebar was more clearly shown at 0.8% and 1.0% fiber mixing ratios due to the strong bonding force at the bonding interface. The bond strength was larger than that of the test sample containing HSF and relatively lower than that of the test sample containing CSF.

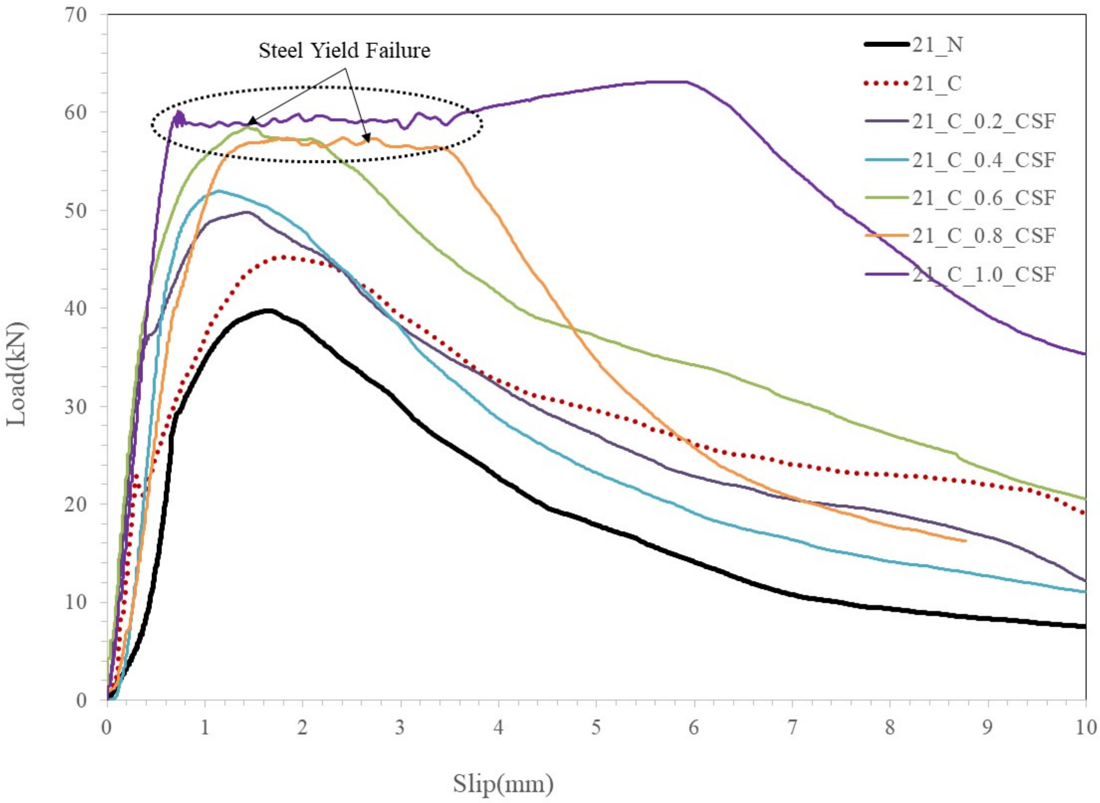

Figure 6. Load–slip curves with crimped steel fiber.

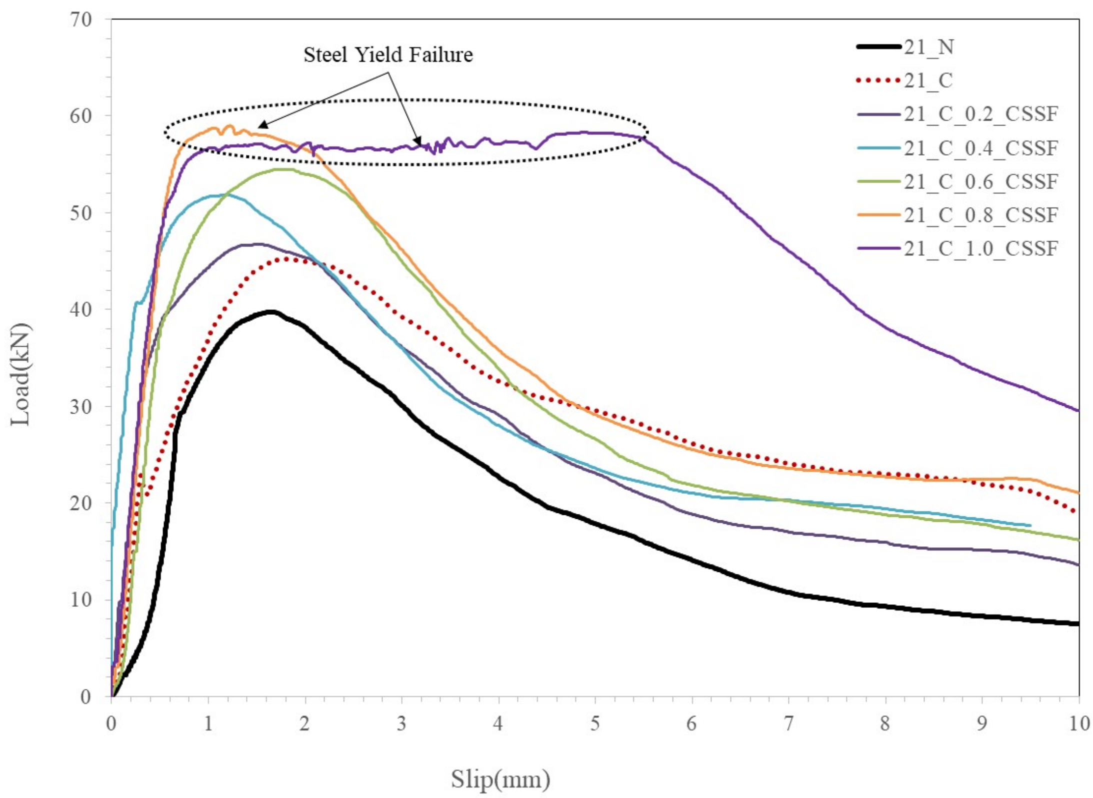

Figure 7. Load–slip curves with crimped stainless steel fiber.

In the pullout resistance curve of the UHPC-coated reinforcing bar, when the initial load was raised, it increased sharply with a small slip. In particular, as the mixing ratio of the fibers increased, the maximum load was reached, with a steep increase in load. At the maximum load, the load gradually decreased due to the pullout phenomenon due to the decrease in the adhesion force, but no abrupt decay was observed after the adhesion failure, as in the case of the sand-coated FRP reinforcing bar [36,40]. It can be judged that the UHPC was strongly attached to the surface of the reinforcing bar (Figure 8), maximizing the resistance to pullout, which did not cause a sudden load reduction after bonding failure at the maximum load. In addition, it seems that the mixing of steel fibers and the increase in the amount strongly improved the pullout resistance.

Figure 8. Examples of failure modes (interface 1 vs. interface 2).

3.2. Bond Strength and Maximum Slip

Figure 9a,b show the bond strength ratio of the uncoated rebars [32] and UHPC-coated rebars, respectively. The bond strength ratio was calculated by dividing the bond strength of each specimen by the average value of the bond strength of uncoated rebar without fiber. For an accurate analysis, the bond strengths of specimens that failed after steel yielding were excluded in the comparison. Figure 9 shows that the bond strengths of uncoated rebars with 1% and 2% fibers increased by 6% and 12.7%, respectively, while those of UHPC-coated rebars with 0.2%, 0.4%, and 0.6% fibers increased by 23.4%, 32.0%, and 40.3%, respectively. The increase rate of the bond strength of the UHPC-coated rebar with a low fiber content was much higher than that of the uncoated rebar with a high fiber content. This means that the UHPC coating promotes the increase in the bond strength of the rebar.

Figure 9b shows that the bond strength of the UHPC-coated rebar increases by about 15 percent compared to the uncoated rebar. Figure 10a,b show the maximum slip ratios of uncoated rebars [32] and UHPC-coated rebars, respectively. The maximum slip ratio was calculated by dividing the slip of each specimen at peak load by the average value of the slip of the uncoated rebar without fiber. Contrary to the change in bond strength ratio, the increase in the slip ratio of the uncoated rebar was greater than that of the UHPC-coated rebars. The slip values of the uncoated rebars with 1% and 2% fibers more than doubled, while those of the UHPC-coated rebars with 0.2%, 0.4%, and 0.6% fibers were almost the same as for the rebar without fiber. This means that the UHPC coating increases the initial bond stiffness of rebar containing fiber, which will be described in detail in the next section.

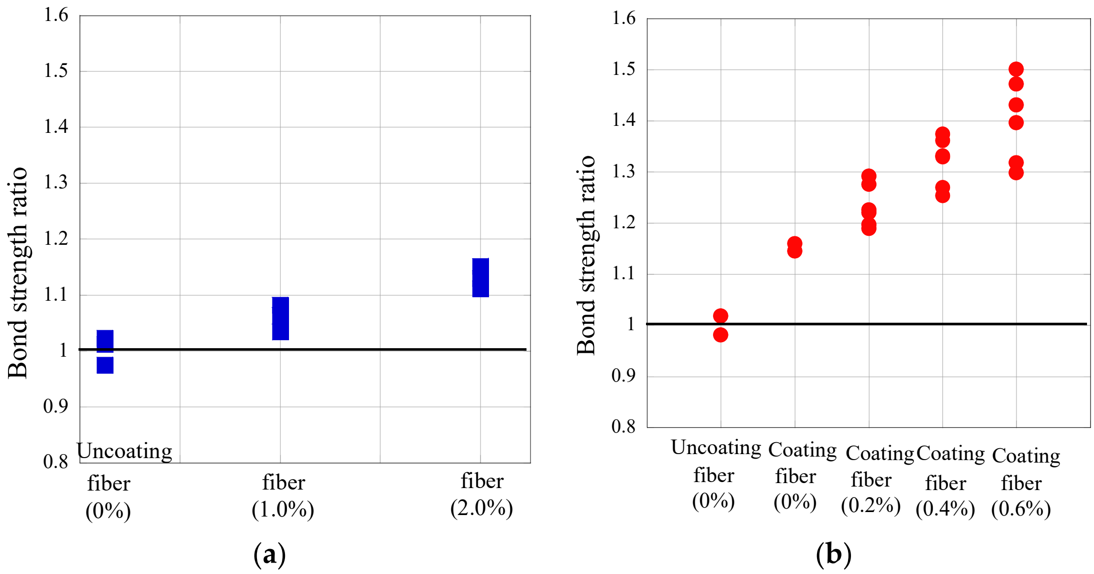

Figure 9. Comparison of the bond strength ratios: (**a**) uncoated rebars [32]; (**b**) UHPC-coated rebars.

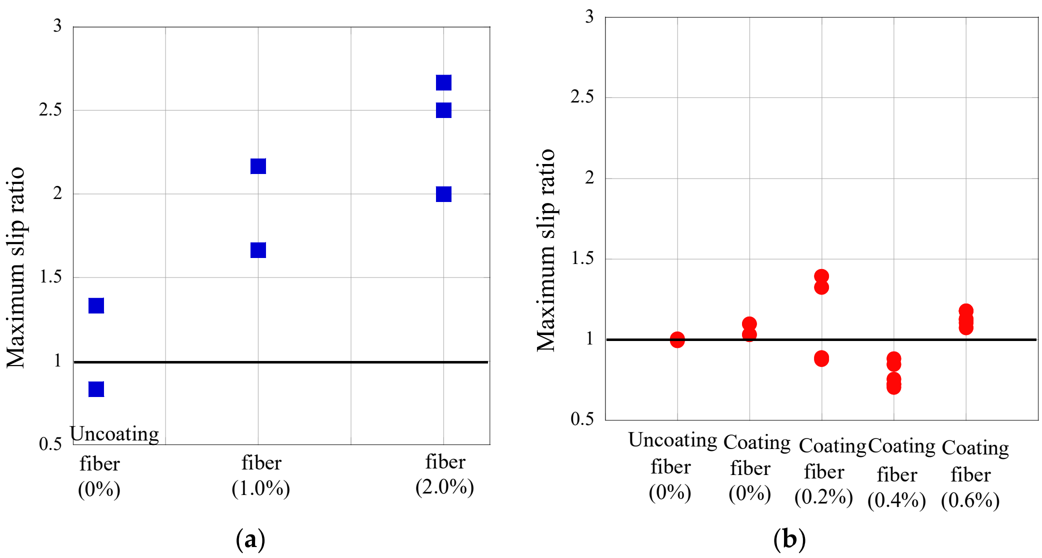

Figure 10. Comparison of the maximum slip ratios at peak load: (**a**) uncoated rebars [32]; (**b**) UHPC-coated rebars.

3.3. Initial Stiffness Influence

The test specimen (21-N) without the UHPC coating on the reinforcing bar's surface showed a large slip with a gradual rising bond stress, regardless of the type of steel fiber.

On the other hand, the test specimen (21-C) reinforced with UHPC between the reinforcing bar and the concrete body showed high initial stiffness due to the strong formation of bonding traction at the interface (Figure 3). In the test specimen reinforced with steel fiber, the overall initial stiffness was greater than that of the simple UHPC-coated rebar. In particular, compared to HSF, the fiber reinforcing effect was more pronounced in the test specimen containing CSF and CSSF, while the change in stiffness was also markedly improved due to the increase in the fiber mixing rate (Figures 5–7). On the other hand, in a study in which a concrete matrix was made with UHPC (f'_c = 200 MPa) and then the rebar pullout test was conducted, the initial stiffness was very strong with zero slippage due to the strong chemical adhesion that occurred until the maximum load was reached [15,41]. In this study, the changes in slippage due to the initial stiffness during the pullout process of UHPC-coated steel rebars reinforced with steel fibers were judged to be greater than that of the specimen reinforced with the UHPC body.

It is known that the fiber content does not affect the initial bond stiffness of the rebar because the fiber plays a role after the rebar has slipped to a certain extent [32]. Since the UHPC increases the bond strength of the rebar but has little effect on slippage, as shown in Figures 9 and 10, the effect of the UHPC coating on the initial bond strength is analyzed in this section. Figure 11 compares the initial bond stiffness ratios of uncoated rebars [32] and UHPC-coated rebars. The initial bond stiffness was calculated by dividing the load of each specimen by the slippage, which corresponded to 40% of the maximum slippage of the uncoated specimen. As shown in Figure 11a, the fiber content does not affect the initial bond stiffness, while the UHPC coating significantly increases the stiffness. Increasing the initial bond stiffness suppresses the bond cracking in the concrete.

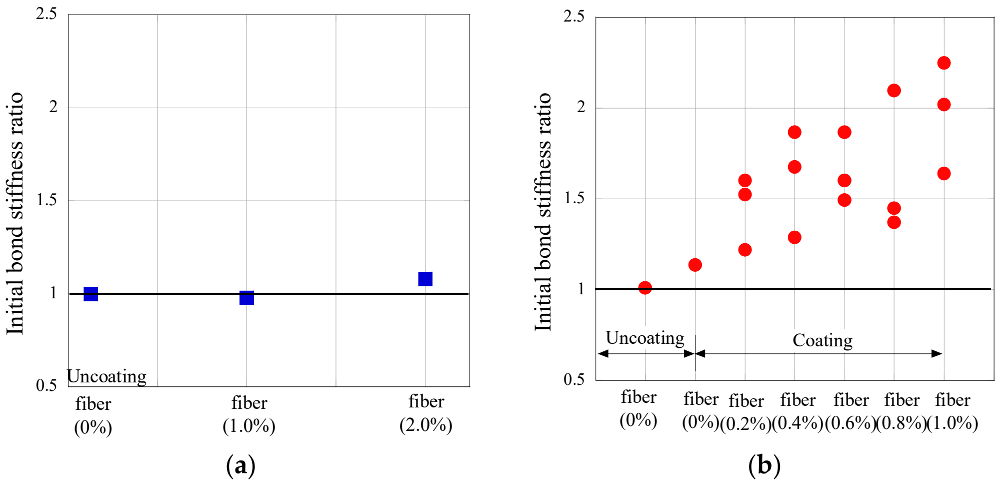

Figure 11. Comparison of the initial bond stiffness ratios: (**a**) uncoated rebars [32]; (**b**) UHPC-coated rebars.

3.4. Analytical Modelling of UHPC-Coated Steel Rebars

3.4.1. Normalized Bond Strength

The normalized bond strength of the steel rebar embedded in ordinary concrete showed a relationship with $\tau_{max} = 2.0 f_c'^{0.5}$ [42]. On the other hand, the normalized bond strength of the steel rebar embedded with UHPFRC exhibited a very high bond strength. The relationship between the bond strength and compressive strength in the study by Yoo et al. [20] was suggested to be $\tau_{max} = 5.0 f_c'^{0.5}$. In this study, a test specimen was prepared using ordinary concrete, with a thin layer of UHPC coated on the steel bar surface, and the change in bond strength was observed by mixing a certain ratio of structural steel fibers into the concrete matrix. As a result of the test, the normalized bond strength increased to about 2.8 in both the specimen simply reinforced with the UHPC coating and the specimen mixed with a certain ratio of steel fibers (Figure 12).

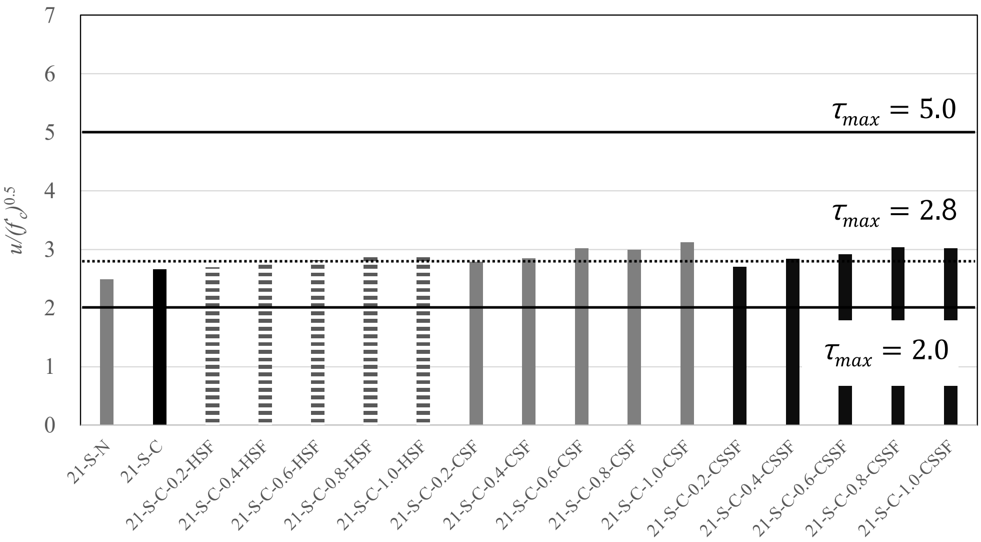

Figure 12. Normalized bond strengths of UHPC-coated steel rebars.

3.4.2. Predicting Bond Stress–Slip Behavior

Bond behaviors between the reinforcing bar and concrete matrix generally describes three kinds of properties [43]. First, the chemical bond created in the interface causes adhesion resistance. Second, the frictional resistance against the slip growth in the interface is created. Third, the irregularity of the interface from the mechanical interlocking attributes to the difference in behavior of the bond–slip curve. In this study, an additional interface from the UHPC coating was created and its effect on the debonding mechanism against the bond–slip behavior was addressed by analyzing previously used bond behavior models. The BPE model [44] for steel bars was developed to explain the bond–slip behavior, as shown in Figure 13:

$$\tau = \tau_{max}\left(\frac{S}{S_1}\right)^{\alpha} \text{ for } S \leq S_1 \quad (3)$$

$$\tau = \tau_{max} \text{ for } S_1 \leq S \leq S_2 \quad (4)$$

$$\tau = \tau_{max} - K_d\,(S - S_2) \text{ for } S_2 < S \leq S_r \quad (5)$$

$$\tau = \tau_r \text{ for } S \geq S_r \quad (6)$$

where τ and S are defined as the bond stress and the corresponding slippage, respectively; α and K_d are the parameters that can be determined from the curve fitting of the experimental results; τ_{max} and τ_r are the maximum bond stress and the residual bond stress, defined as the bond stress and the corresponding slippage, respectively; S_1, S_2, and S_r are the corresponding slippage values for the maximum bond stress, the border of the maximum bond stress plateau, and the residual bond stress, respectively. The other model for representing the bond–slip behavior is the CMR model [45], defined as:

$$\tau = \tau_{max}\left(1 - e^{\frac{-s}{s_r}}\right)^{\beta} \textbf{ for } S \leq S_1 \quad (7)$$

where s_r and β are parameters that can be determined from the curve fitting coefficients. Figure 14 compares the results of the predicted BPE and CMR models with the experimental bond–slip behavior. The increase in the structural steel fibers reduced the slippage at the maximum load and increased the maximum bond stress. The predicted CMR models proposed by Cosenza et al. [45] matched well with the bond stress–slip response for the UHPC-coated steel rebars. The results using UHPC as a concrete matrix agreed well with the results reported by Yoo et al. [15]. The difference from Yoo et al.'s results was that the UHPC was thinly coated on the steel rebar or composed the entire matrix. It was judged that the experimental value from the CMR model was predicted well, regardless of the composition of the concrete matrix in the section where the maximum load was reached. The parameters used for predicting BPE and CMR models are arranged in Table 6.

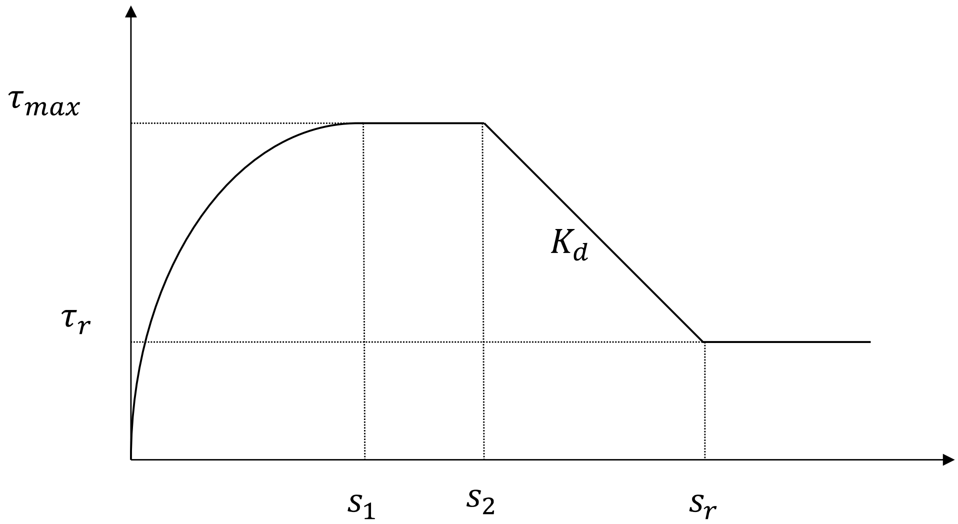

Figure 13. BPE model of the bond–slip curve for the steel rebar.

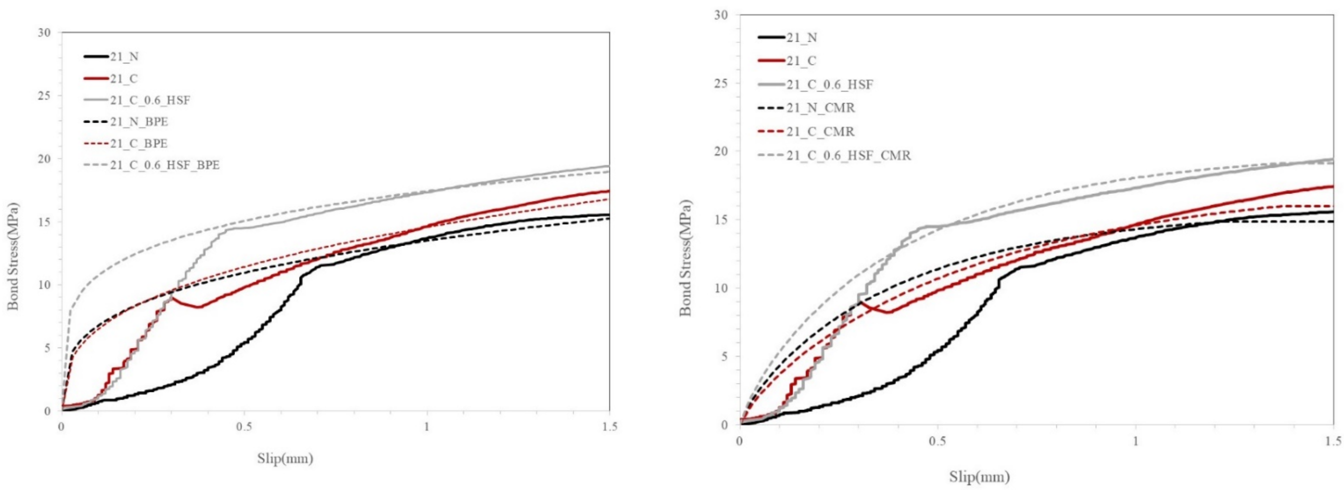

(**a**) (**b**)

Figure 14. Comparison of BPE (a) and CMR (b) models for steel rebar coated and reinforced with UHPC.

The slip values (S_1, S_2) corresponding to 95% of the maximum bond stress were determined to define the second stage of the BPE model using Equation (8) by considering the effects of the UHPC coating and steel fiber volume in the concrete matrix. These points represent the borders between stage 1 and stage 2 as well as stage 2 and stage 3. The parameters of the proposed stages 2–4 (Equations (9) and (10)) were calculated and are reported in Table 7. Figure 15 presents a proposed model from the ascending stage to final the stage for the pullout behavior of the UHPC-coated steel rebar, while Figure 16 shows the predicted pullout curve compared to the experimental results for all specimens.

Table 6. Parameters for the ascending parts of existing models.

Specimen	τ_{max} (MPa)	S_m (mm)	BPE	CMR	
			α	β	S_r
21-N	15.40	1.63	0.30	0.80	0.45
21-C	17.76	1.74	0.35	0.80	0.67
21-C-0.2-HSF	18.56	2.22	0.33	0.80	0.65
21-C-0.4-HSF	19.44	1.41	0.25	0.80	0.50
21-C-0.6-HSF	20.15	1.86	0.21	0.80	0.47
21-C-0.8-HSF	20.75	1.49	0.20	0.80	0.43
21-C-1.0-HSF	21.11	1.80	0.18	0.80	0.41
21-C-0.2-CSF	19.78	1.44	0.28	0.80	0.52
21-C-0.4-CSF	20.84	1.17	0.22	0.80	0.25
21-C-0.6-CSF	22.89	1.80	0.27	0.80	0.55
21-C-0.8-CSF	22.90	0.80	0.06	0.80	0.22
21-C-1.0-CSF	24.86	0.88	0.09	0.80	0.42
21-C-0.2-CSSF	18.66	0.52	0.30	0.80	0.33
21-C-0.4-CSSF	20.72	1.20	0.28	0.80	0.30
21-C-0.6-CSSF	21.77	1.88	0.25	0.80	0.28
21-C-0.8-CSSF	23.02	1.20	0.23	0.80	0.25
21-C-1.0-CSSF	23.19	0.72	0.15	0.80	0.16

$$\tau = 0.95\tau_{max} \text{ for } S_1 \leq S = V_f S_{max} \leq S_2 \tag{8}$$

$$\tau = 0.95\tau_{max} - K_d\ (S - S_2) \text{ for } S_2 < S \leq S_r \tag{9}$$

$$\tau = \tau_r \text{ for } S \geq S_r \tag{10}$$

Table 7. Experimental results of the proposed model.

Specimen	$0.95\tau_{max}$ (MPa)	S_1	S_2	K_d (MPa/mm)	τ_r (MPa)
21-N	14.10	1.22	2.07	3.20	4.94
21-C	16.96	1.37	2.52	3.91	5.81
21-C-0.2-HSF	17.40	1.65	2.78	2.78	6.30
21-C-0.4-HSF	18.59	0.93	1.90	5.12	6.26
21-C-0.6-HSF	19.00	1.37	2.59	3.74	7.11
21-C-0.8-HSF	19.83	1.22	2.01	4.97	7.21
21-C-1.0-HSF	20.01	1.25	2.34	3.96	7.76
21-C-0.2-CSF	18.67	0.92	1.85	5.10	6.27
21-C-0.4-CSF	19.49	0.82	1.81	7.65	7.02
21-C-0.6-CSF	21.96	1.02	2.32	5.01	7.26
21-C-0.8-CSF	21.53	1.15	3.64	3.96	9.80
21-C-1.0-CSF	23.67	0.73	5.70	4.81	7.34
21-C-0.2-CSSF	17.52	1.00	2.18	8.13	9.97
21-C-0.4-CSSF	19.46	0.67	1.63	3.80	12.17
21-C-0.6-CSSF	20.43	1.19	2.43	2.91	8.19
21-C-0.8-CSSF	22.13	0.70	2.05	4.08	13.86
21-C-1.0-CSSF	21.86	0.78	4.87	2.02	12.48

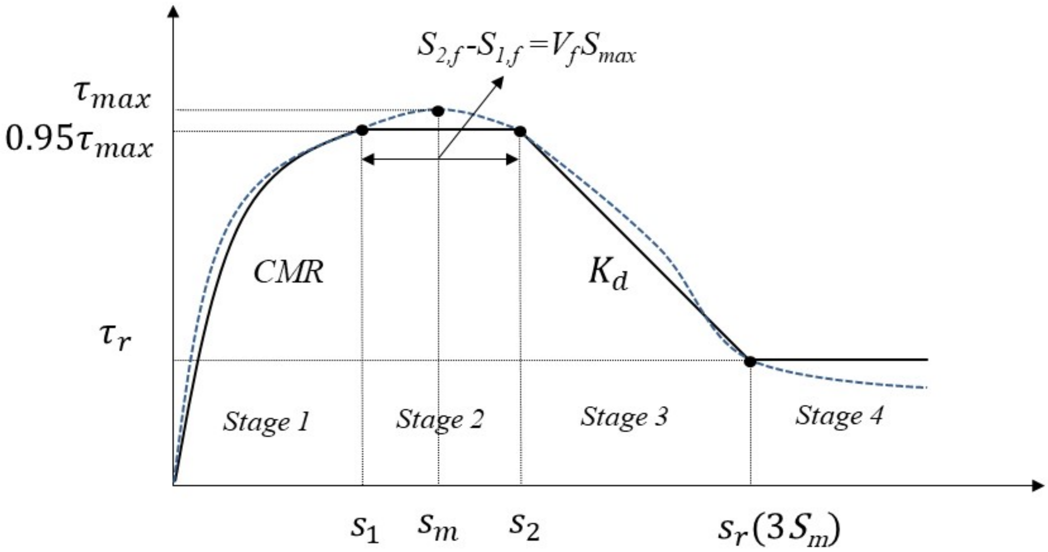

Figure 15. Proposed model for UHPC-coated steel rebar.

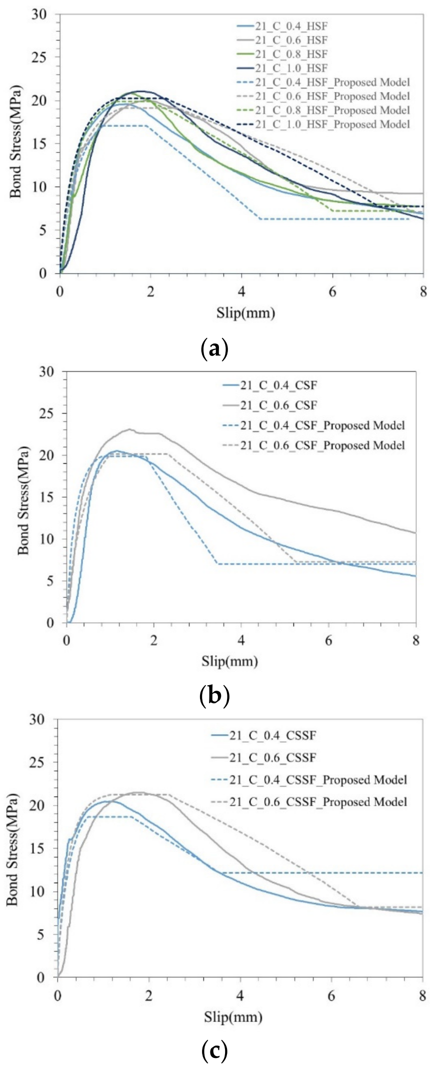

Figure 16. Proposed model for steel rebars coated with UHPC and (**a**) HSF, (**b**) CSF, or (**c**) CSSF.

The prediction models for the bond–slip behavior of UHPC-coated steel rebars with the addition of different steel fibers into the concrete matrix offered reasonable prediction results. The ascending branches before the maximum load were predicted using the CMR model (Equation (7)) and BPE model (Equations (8)–10)), which were modified and applied to predict the post-behavior after the maximum load.

4. Conclusions

The application of ultra-high-performance concrete for conventional steel rebar has a great effect on the improvement of the bond–slip behavior. The excellent surface bonding with minimized porosity on the steel rebar caused a significant change in the de-bonding mechanism before and after the maximum load. Based on the results of the experimental study, we proposed reasonable prediction models of the monotonic bond performance by applying existing models. The following conclusions can be drawn:

1. The thin layer of UHPC coating on the surface was strongly attached to the reinforcing bar and bond failure due to slippage was observed at the UHPC-OPC interface (interface 2) by inducing the integral behavior;
2. The UHPC-coated reinforcing bar significantly improved the bond strength and pullout performance by forming a new interface, while the addition of steel fibers improved the overall performance of the adhesion–slip behavior. Among the fiber types, the crimped steel fiber had the highest effect on the bond performance;
3. The bond failure modes were sensitive to the thin coating of UHPC, creating an additional interface between the steel rebar and concrete matrix. Most of specimens had high residual bond stresses compared to the control specimen. For the 0.8% and 1.0% fiber volumes in both CSF and CSSF specimens, the strain hardening of the steel rebar against the pullout load was created, which delayed the bonding failure mechanism;
4. The prediction models were proposed by analyzing existing models (BPE, CMR). The CMR model fitted the ascending branches well compared to the BPE model before the maximum load. After the maximum load, a prediction model for the residual load was proposed by modifying the existing BPE model through a comparison with the experimental data.

Author Contributions: B.K., I.-H.E. and S.-K.O. conceived and designed the experiments. I.-H.E. and B.K. performed the experiments. S.-K.O., B.K. and I.-H.E. analyzed the data. B.K., I.-H.E. and S.-K.O. wrote the paper. All authors have read and agreed to the published version of the manuscript.

Funding: This study was financially supported by the Seoul National University of Science and Technology.

Institutional Review Board Statement: Not applicable.

Informed Consent Statement: Not applicable.

Conflicts of Interest: The authors declare no conflict of interest.

References

1. Lee, J.Y. *Reinforced Concrete Structure*; Donghwa: Paju, Korea, 2011; pp. 20–26.
2. Mindess, S.; Young, J.F.; Darwin, D. *Concrete*; Prentice Hall: Hoboken, NJ, USA, 2003; pp. 477–498.
3. Oh, B.H. Pull-out bond characteristics of reinforced concrete members. *Korea Concr. Inst.* **1992**, *4*, 113–121.
4. Oh, B.H.; Kang, Y.J.; Lee, S.R.; Bang, K.S. An experimental study on the bond characteristics of reinforced concrete structures. *Korea Concr. Inst.* **1990**, *4*, 99–107.
5. Ferguson, P.M.; Thomson, N. Development length of high strength reinforcing bars in bond. *ACI J.* **1962**, *59*, 887–923.
6. Losberg, A.; Olsson, P.A. Bond failure of deformed reinforcing bars based on the longitudinal splitting effect of the bars. *ACI J.* **1979**, *76*, 5–19.
7. Thompson, M.A.; Jirsa, J.O.; Breen, J.E.; Meinheit, D.F. Behavior of multiple lap splices in wide section. *ACI J.* **1979**, *76*, 227–248.
8. Chung, H.W. Epoxy repair of bond in reinforced concrete members. *ACI J.* **1981**, *78*, 79–85.
9. Edwards, A.D.; Yannopoulos, P.J. Local bond stress to slip relationships for hot rolled deformed bars and mild steel plain bars. *ACI J.* **1979**, *76*, 405–421.

10. Yoo, D.-Y.; Kwon, K.-Y.; Park, J.-J.; Yoon, Y.-S. Local bond-slip response of GFRP rebar in ultra-high-performance fiber-reinforced concrete. *Compos. Struct.* **2015**, *120*, 53–64. [CrossRef]
11. Zhou, M.; Lu, W.; Song, J.; Lee, G.C. Application of Ultra-High Performance Concrete in bridge engineering. *Constr. Build. Mater.* **2018**, *186*, 1256–1267. [CrossRef]
12. Xue, J.; Briseghella, B.; Huang, F.; Nuti, C.; Tabatabai, H.; Chen, B. Review of ultra-high performance concrete and its application in bridge engineering. *Constr. Build. Mater.* **2020**, *260*, 119844. [CrossRef]
13. Shi, C.; Wu, Z.; Xiao, J.; Wang, D.; Huang, Z.; Fang, Z. A review on ultra high performance concrete: Part I. Raw materials and mixture design. *Constr. Build. Mater.* **2015**, *101*, 741–751. [CrossRef]
14. Wang, D.; Shi, C.; Wu, Z.; Xiao, J.; Huang, Z.; Fang, Z. A review on ultra high performance concrete: Part II. Hydration, microstructure and properties. *Constr. Build. Mater.* **2015**, *96*, 368–377. [CrossRef]
15. Bae, Y.; Pyo, S. Ultra high performance concrete (UHPC) sleeper: Structural design and performance. *Eng. Struct.* **2020**, *210*, 110374. [CrossRef]
16. Bae, Y.; Pyo, S. Effect of steel fiber content on structural and electrical properties of ultra high performance concrete (UHPC) sleepers. *Eng. Struct.* **2020**, *222*, 111131. [CrossRef]
17. Brühwiler, E.; Denarié, E. Rehabilitation and Strengthening of Concrete Structures Using Ultra-High Performance Fibre Reinforced Concrete. *Struct. Eng. Int.* **2013**, *23*, 450–457. [CrossRef]
18. Yoo, D.-Y.; Lee, J.-H.; Yoon, Y.-S. Effect of fiber content on mechanical and fracture properties of ultra high performance fiber reinforced cementitious composites. *Compos. Struct.* **2013**, *106*, 742–753. [CrossRef]
19. Richard, P.; Cheyrezy, M. Composition of reactive powder concretes. *Cem. Concr. Res.* **1995**, *25*, 1501–1511. [CrossRef]
20. Yoo, D.-Y.; Shin, H.-O.; Yang, J.-M.; Yoon, Y.-S. Material and bond properties of ultra high performance fiber reinforced concrete with micro steel fibers. *Compos. Part B Eng.* **2014**, *58*, 122–133. [CrossRef]
21. De Larrard, F.; Sedran, T. Optimization of ultra-high-performance concrete by the use of a packing model. *Cem. Concr. Res.* **1994**, *24*, 997–1009. [CrossRef]
22. Meng, W.; Khayat, K.H. Mechanical properties of ultra-high-performance concrete enhanced with graphite nanoplatelets and carbon nanofibers. *Compos. Part B Eng.* **2016**, *107*, 113–122. [CrossRef]
23. Habel, K.; Viviani, M.; Denarié, E.; Brühwiler, E. Development of the mechanical properties of an Ultra-High Performance Fiber Reinforced Concrete (UHPFRC). *Cem. Concr. Res.* **2006**, *36*, 1362–1370. [CrossRef]
24. Yu, R.; Spiesz, P.; Brouwers, H.J.H. Mix design and properties assessment of Ultra-High Performance Fibre Reinforced Concrete (UHPFRC). *Cem. Concr. Res.* **2014**, *56*, 29–39. [CrossRef]
25. Schröfl, C.; Gruber, M.; Plank, J. Preferential adsorption of polycarboxylate superplasticizers on cement and silica fume in ultra-high performance concrete (UHPC). *Cem. Concr. Res.* **2012**, *42*, 1401–1408. [CrossRef]
26. Dingqiang, F.; Yu, R.; Kangning, L.; Junhui, T.; Zhonghe, S.; Chunfeng, W.; Shuo, W.; Zhenfeng, G.; Zhengdong, H.; Qiqi, S. Optimized design of steel fibres reinforced ultra-high performance concrete (UHPC) composites: Towards to dense structure and efficient fibre application. *Constr. Build. Mater.* **2020**, *273*, 121698. [CrossRef]
27. Naaman, A.E.; Reinhardt, H.W. Proposed classification of HPFRC composites based on their tensile response. *Mater. Struct.* **2006**, *39*, 547–555. [CrossRef]
28. Jungwirth, J.; Muttoni, A. Structural behavior of tension members in UHPC. In *Proceedings of the International Symposium on Ultra High Performance Concrete*; Springer: Kassel, Germany, 2004; pp. 533–544.
29. Yang, I.H.; Joh, C.; Kim, B.-S. Structural behavior of ultra high performance concrete beams subjected to bending. *Eng. Struct.* **2010**, *32*, 3478–3487. [CrossRef]
30. Graybeal, B.A. Flexural Behavior of an Ultrahigh-Performance Concrete I-Girder. *J. Bridg. Eng.* **2008**, *13*, 602–610. [CrossRef]
31. Branson, A.K. Precast Bridge Deck Joints Using FRP and Ultra-High Performance Concrete. Master's Thesis, The University of Western Ontario, London, ON, Canada, 2013; pp. 1–132.
32. Kim, B.; Lee, J.Y. Polyvinyl alcohol engineered cementitious composite (PVA-ECC) for the interfacial bond behavior of glass fibre reinforced polymer bars (GFRP). *Polym. Polym. Compos.* **2012**, *20*, 545–557.
33. Lee, J.; Yi, C.; Kim, B.; Cheong, Y. Bond degradation of glass fibre reinforced plastic bars in concrete subjected to tensile cyclic loads. *J. Reinf. Plast. Compos.* **2013**, *32*, 463–475. [CrossRef]
34. Lee, J.Y.; Yi, C.K.; Cheong, Y.G.; Kim, B.I. Bond stress–slip behaviour of two common GFRP rebar types with pullout failure. *Mag. Concr. Res.* **2012**, *64*, 575–591. [CrossRef]
35. Kim, B.; Lee, J.-Y. Resistance of interfacial debonding failure of GFRP bars embedded in concrete reinforced with structural fibers under cycling loads. *Compos. Part B Eng.* **2018**, *156*, 201–211. [CrossRef]
36. Yoo, D.-Y.; Park, J.-J.; Kim, S.-W.; Yoon, Y.-S. Influence of reinforcing bar type on autogenous shrinkage stress and bond behavior of ultra high performance fiber reinforced concrete. *Cem. Concr. Compos.* **2014**, *48*, 150–161. [CrossRef]
37. Ametrano, D. Bond Characteristics of Glass Fibre Reinforced Polymer Bars Embedded in High Performance and Ultra-High Performance Concrete. Master's Thesis, Ryerson University, Toronto, ON, Canada, 2011; pp. 1–132.
38. Hossain, K.M.; Ametrano, D.; Mak, C.; Lachemi, M. *Bond Strength and Development Length of GFRP Bars in Ultra-High Performance Concrete*; Materials Engineering and Research Office Report; Ontario Ministry of Transportation: Toronto, ON, Canada, 2011; pp. 1–96.

39. Alavi-Fard, M.; Marzouk, H. Bond behavior of high strength concrete under reversed pull-out cyclic loading. *Can. J. Civ. Eng.* **2002**, *29*, 191–200. [CrossRef]
40. Baean, M.; Torres, L.; Turon, A.; Barris, C. Experrimental study of bond behavior between concrete and FRP bars using a pull-out test. *Compos. Part B* **2009**, *40*, 784–797. [CrossRef]
41. Lee, J.-Y.; Kim, T.-Y.; Yi, C.-K.; Park, J.-S.; You, Y.-C.; Park, Y.-H. Interfacial bond strength of glass fiber reinforced polymer bars in high-strength concrete. *Compos. Part B Eng.* **2008**, *39*, 258–270. [CrossRef]
42. CEM Bulletins. *CEB-FIP Model Code for Concrete Structures*; Comite Euro International du Beton: Lausanne, Switzerland, 1993.
43. ACI Committee. *Bond and Development of Straight Reinforcing Bars in Tension*; ACI 408R-03; American Concrete Institute: Detroit, MI, USA, 2003.
44. Eligehusen, R.; Popve, E.P.; Bertero, V.V. *Local Bond Stress-Slip Relationships of Deformed Bars under Generalized Excitations*; University of California: Berkeley, CA, USA, 1982.
45. Cosenza, E.; Manfredi, G.; Realfonzo, R. Analytical modelling of bond between FRP reinforcing bars and concrete. In *Proceedings of the Second International RILEM Symposium (FRPRCS-2)*; Taerwe, L., Ed.; E. and F.N. Spon: London, UK, 1995; pp. 164–171.